Carbohydrate Polymers 111 (2014) 734–743

Contents lists available at ScienceDirect

Carbohydrate Polymers

journal homepage: www.elsevier.com/locate/carbpol

One pot green synthesis of Ag, Au and Au–Ag alloy nanoparticles using *isonicotinic acid hydrazide* and starch

Sampath Malathi [1], Tamilarasu Ezhilarasu [1], Tamilselvan Abiraman [1], Sengottuvelan Balasubramanian *

Department of Inorganic Chemistry, University of Madras, Guindy Campus, Chennai 600 025, Tamilnadu, India

ARTICLE INFO

Article history:
Received 21 March 2014
Received in revised form 24 April 2014
Accepted 28 April 2014
Available online 20 May 2014

Keywords:
Silver
Gold
Alloy nanoparticles
Isoniazid
Cyclic voltammetry
4-Nitrophenol

ABSTRACT

Gold–silver alloy nanoparticles were synthesized via chemical reduction of varying mole fractions of chloroauric acid ($HAuCl_4$) and silver nitrate ($AgNO_3$) by environmentally benign *isonicotinic acid hydrazide* (INH) in the presence of starch as a capping agent in aqueous medium. The absorption spectra of Au–Ag nanoparticles show blue shift with increasing silver content indicating the formation of alloy nanoparticles. When the Ag content in the alloy decreases the size of the nanoparticles increases and as a result of which the oxidation potential also increases. The emission maximum undergoes a red shift from 443 to 614 nm. The nanoparticles are monodisperse and spherical with an average particle size of 3–18 nm. The catalytic behavior of alloy nanoparticles indicate that the rate constant for the reduction of 4-nitro phenol to 4-amino phenol increases exponentially from metallic Ag to metallic Au as Au content increases in the Au–Ag alloy nanoparticles.

1. Introduction

Metal nanoparticles show characteristic size-dependent properties different from those of bulk metals with significant size effects occurring in 1–10 nm diameter range (Link, Burda, Wang, & El-Sayed, 1999a; Link, Wang, & El-Sayed, 1999b). Au–Ag NPs with certain bimetallic compositions have been synthesized in single-phase (water) (Mallin & Murphy, 2002) as well as in bi-phasic (toluene–water) (Hostetler et al., 1998) medium. Au–Ag alloy nanoparticles have been synthesized by $NaBH_4$ reduction of supported metal salts (Kim, Kim, Kim, & Yoo, 2013), citrate reduction (Link et al., 1999b), hydrazine reduction (Chen & Chen, 2002), laser ablation (Liz-Marzan & Philipse, 1995), sputter deposition (Okazaki et al., 2008), laser irradiation (Chen & Yeh, 2001), sonochemical method (Anandan, Grieser, & Ashokkumar, 2008) and also by biosynthesis (Senapati, Ahmad, Khan, Sastry, & Kumar, 2005). Kim et al. have reported the synthesis of Au–Ag alloy nanoparticles by laser ablation of bulk alloys (Lee, Han, & Kim, 2001). Teo, Keating, and Kao (1987) have synthesized 38 atom gold–silver clusters (Au_{18} Ag_{20}) to investigate the minimum number of atoms in a cluster required to exhibit metallic behavior.

The alloy NPs with smaller sizes are often required in the field of catalysis due to their higher activity (Zhang, Zhang, Wei, Du, & Li, 2009). For example, sub-5 nm Au–Ag alloy NPs strongly enhanced oxidation of carbon monoxide, which could be prepared by half-seeding or a templating approach (Wang, Liu, Lin, Lin, & Mou, 2005). However, the complex experimental procedures of such methods restricted their practical applications. Therefore, it is necessary to develop a facile method for the preparation of high quality Au–Ag alloy NPs with smaller size in the solution phase.

4-Pyridine carboxylic acid hydrazide (INH) possesses significant physiological activities among the three isomeric 2, 3 and 4-pyridine carboxylic acid hydrazides. INH via passive diffusion rapidly permeates the bacterial cell membrane wherein the hydrazide group in the molecule serves only as a carrier group (Kruger–Thiemer) (Kruger–Thiemer, 1955). INH has been the accepted drug for use as TB prophylaxis in immunocompetent as well as in HIV positive cases (Carosi & Matteelli, 1996). The transition metal complexes of INH exhibit interesting biological activities. The catalytic conversion of epoxides into ninhydrins is possible with this compound (Sharghi, Eskandari, & Ghavami, 2004) and it has been found to act as a molecular logic gate in aqueous medium (Magria & Prasanna de Silva, 2010).

The objective of this study is to develop a simple one-step and "green" approach to synthesize Au, Ag and Au–Ag alloy nanoparticles by chemical reduction using isonicotinic acid hydrazide (Isoniazid) and starch as the capping agent. Isoniazid is being used

* Corresponding author. Tel.: +91 4422202794.
E-mail address: bala2010@yahoo.com (S. Balasubramanian).
[1] Tel.: +91 4422202794.

http://dx.doi.org/10.1016/j.carbpol.2014.04.105
0144-8617/

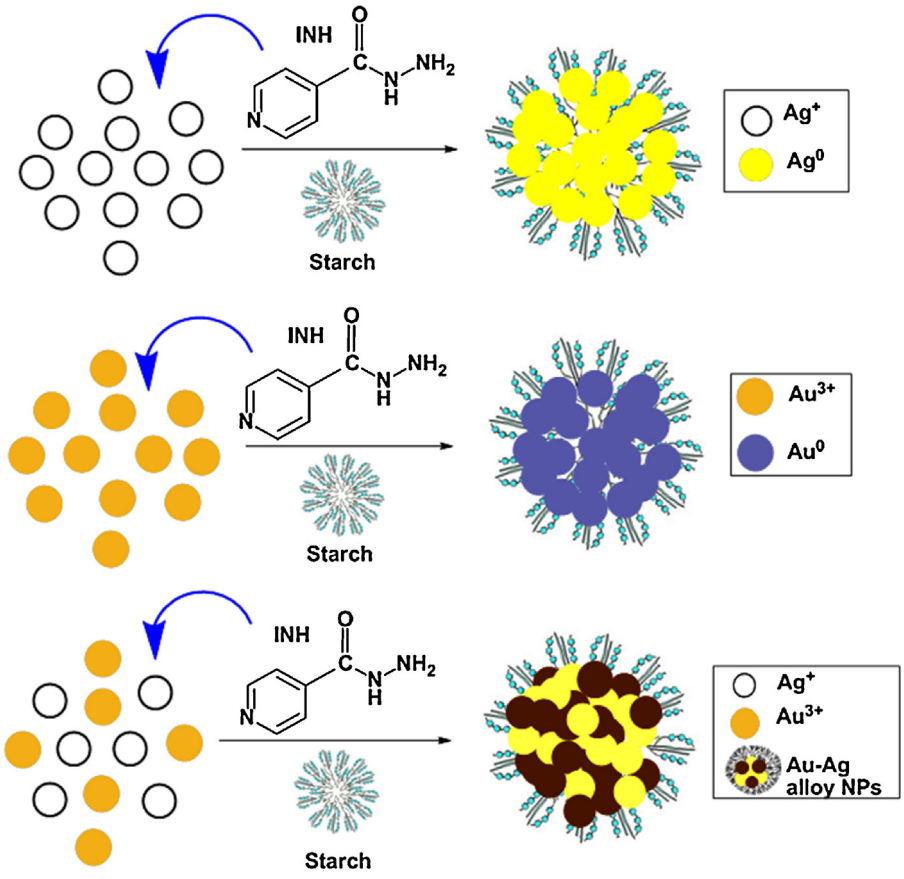

Scheme 1. Schematic illustration of Ag, Au, Au–Ag alloy nanoparticles.

as a first line anti-tuberculosis drug (Winder, 1956). The byproduct isonicotinic acid produced in this reaction is also non-toxic and eco-friendly. The homogeneous Au–Ag alloy nanoparticles prepared in this study can be used as a catalyst for the reduction of 4-nitrophenol and picric acid in presence of $NaBH_4$ for the synthesis of amino phenols. The amino phenol is an important intermediate in the manufacture of many analgesic and antipyretic drugs besides its application as photographic developer, corrosion inhibitor and hair dyeing agent (Corbett, 1999).

2. Experimental

2.1. Materials

Chloroauric acid ($HAuCl_4{\cdot}xH_2O$, LR, LOBA Chemie, India), silver nitrate ($AgNO_3$, AR, BDH, India), 4-nitrophenol ($C_6H_5NO_3$, AR, SRL, India), sodium borohydride ($NaBH_4$, LR, Merck, India), picric acid ($C_6H_3N_3O_7$, AR, BDH, India) isoniazid ($C_6H_7N_3O$, AR, Fluka, India) and starch [$(C_6H_{10}O_5)_n$, soluble GR, Merck, India] were used as such without further purification. Milli-Q water was used throughout the experiment.

2.2. Methods

2.2.1. Synthesis of silver nanoparticles, gold nanoparticles and Au–Ag alloy nanoparticles

20 mL aqueous solution containing starch (1%) and $AgNO_3$ (0.1 mM) was taken in a round bottom flask and 0.025 mM (2.5 mL) of freshly prepared aqueous isoniazid solution was added to it. The mixture was heated to 60 °C with continuous stirring till the solution turns yellow indicating the formation of AgNPs. Similarly a solution containing $HAuCl_4{\cdot}xH_2O$ (0.1 mM) and starch (1%) was taken in a round bottom flask. The mixture was stirred continuously at room temperature, followed by the dropwise addition of isoniazid (0.025 mM). The solution turns purple indicating the formation of AuNPs. Au–Ag alloy nanoparticles were synthesized by the reduction of $HAuCl_4{\cdot}xH_2O$ and $AgNO_3$ with isoniazid in the presence of starch with varying initial Au–Ag molar ratios (1:0, 0.75:0.25, 0.50:0.50, 0.25:0.75 and 0:1). The resultant 0.50:0.50 Au–Ag solution consists of 10 mL of 1% starch, 2.5 mL (0.1 mM) $HAuCl_4{\cdot}xH_2O$ and 2.5 mL (0.1 mM) $AgNO_3$. 5.0 mL of an aqueous solution of (0.025 mM) isoniazid was added all at once with vigorous stirring. The solution was allowed to stir for an additional 60 s. The color of the resulting nanoparticle solution depends on the initial composition of Au–Ag alloy nanoparticles. The resulting nanoparticles were analyzed by UV–visible spectrophotometry (Scheme 1).

2.2.2. Catalytic reduction of 4-nitrophenol

0.25 mL of 10 mM aqueous solution of 4-nitrophenol and 0.25 mL of 1 M freshly prepared aqueous solution of $NaBH_4$ were mixed with 2.5 mL of Milli-Q water at room temperature. 100 μL of 0.1 mM Au, Ag, Au–Ag alloy nanoparticles were mixed with the above solution and UV–visible absorption spectra were recorded with time to monitor the change in the reaction mixture. The above procedure is also followed for the reduction of picric acid with or without the presence of the nanoparticles (Scheme 2).

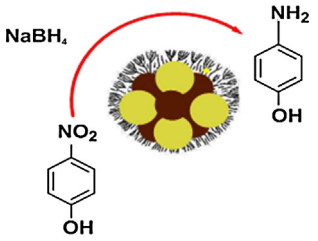

Scheme 2. Catalytic reduction of 4-nitrophenol.

2.2.3. Fabrication of silver, gold, and their alloy nanoparticles modified GCE

The CV (cyclic voltammetry) studies were carried out on a CH Instruments Model CHI-1130A electrochemical workstation (USA). The three electrode cell assembly consists of the bare GCE as well as modified by metal/alloy nanocoating as working electrode, platinum wire as counter electrode and Ag/AgCl as reference electrode. The experiments were conducted in PBS (pH: 7.4) medium and 3 M KCl as supporting electrolyte. The solution was purged by N_2 gas to remove the dissolved oxygen. The potential was scanned between 1 V and −1 V at a scan rate of 50 mV s^{-1}. The nanoparticles coated GCE electrode was fabricated individually by casting 10 μL of each nanoparticle solution. Then the solvent was allowed to dry at room temperature and rinsed with water in order to remove any loosely bound nanoparticles.

2.2.4. Characterization

The aqueous solution of monometallic and bimetallic nanoparticles were examined using Ultraviolet–visible spectrophotometer (Perkin-Elmer, λ 35, USA) in the range of 200–800 nm. Transmission electron microscopic (TEM) studies were carried out using TECNAI, G2-MODEL, T-30 S-TWIN with an acceleration voltage of 250 kV. The aqueous solution of nanoparticles was drop cast onto a carbon-coated copper grid sample holder followed by evaporation at room temperature. The size distribution of the nanoparticles was estimated based on images J software (version 1.47). The X-ray photoelectron spectroscopy (XPS) measurements were made on a Physical Electronics-Quantum 2000 EAC (SPHERA 547) scanning microprobe. This system uses a focused monochromatic Al Kα X-ray (1486.7 eV) source for excitation, a spherical section analyzer and a seven channel detection system. The fluorescence measurement was carried out at room temperature using a Varian–Cary Eclipse fluorescence spectrophotometer. The fluorescence measurements were carried out in the range 350–700 nm.

3. Results and discussion

The green synthesis of AgNPs was achieved by chemical reduction of silver ions using INH as a reducing agent and starch as a capping agent. In this study, starch is used as a template for nanoparticle growth while INH serves as an environmentally benign reducing agent for the reduction of silver ions. The silver nanoparticle solution shows an absorption maximum at 411 nm. While mild heating is sufficient for the INH reduction of silver ions, the reduction of Au^{3+} ions of $HAuCl_4$ occurs at room temperature.

The surface plasmon absorption maximum of the purple color AuNPs, which is obtained from 0.1 mM solution of Au^{3+} ions, is 576 nm. The reduction of Au^{3+} ions occurs fairly rapidly and more than 90% of Ag^+ and Au^{3+} ions are reduced within 15 min and 2 min respectively, after the addition of INH to the metal ion solution. The comparatively slower reduction rate of silver ions relative to that of gold ions is most likely due to differences in the reduction potentials of the two metal ions, the redox potential being considerably lower for Ag^+ to Ag^0 (Raveendran, Fu, & Wallen, 2003). INH is considered to be "greener" in terms of biocompatibility and starch is one of the polysaccharides, which belongs to the most abundant natural and renewable biopolymers. The hydroxyl groups of starch help to protect the surface of these particles in the absence of which they will aggregate as a result of high surface energies. Starch serves as a stabilizing template for the alloy nanoparticles (Hussain, Kumar, Hashmi, & Khan, 2011).

The synthesis of Ag, Au and Au–Ag alloy nanoparticles is very simple. The mixtures of Ag and Au metal ion solution containing starch undergo change in color upon addition of INH depending on the molar composition of Ag and Au. The $AgNO_3$ solution changes from colorless to yellow upon reduction. However, as the Au content increases, the intensity of the purple color increases (Vide: Supporting Fig. S1). This is the first report where NPs of Ag, Au and Au–Ag from Ag^+ and Au^{3+} ions are prepared using INH as a reducing agent. The Au–Ag alloy nanoparticles, as well as Ag and Au nanoparticles, can be characterized by UV–visible absorption spectroscopy. Silver and gold nanoparticles are known to exhibit surface plasmon resonance bands in the visible region at ~440 nm (Naik, Stringer, Agarwal, Jones, & Stone, 2002) and ~530 nm (Aryal et al., 2006), respectively. The UV–visible spectra of the Ag and Au NPs prepared from the salts of the metals exhibit distinct peaks at

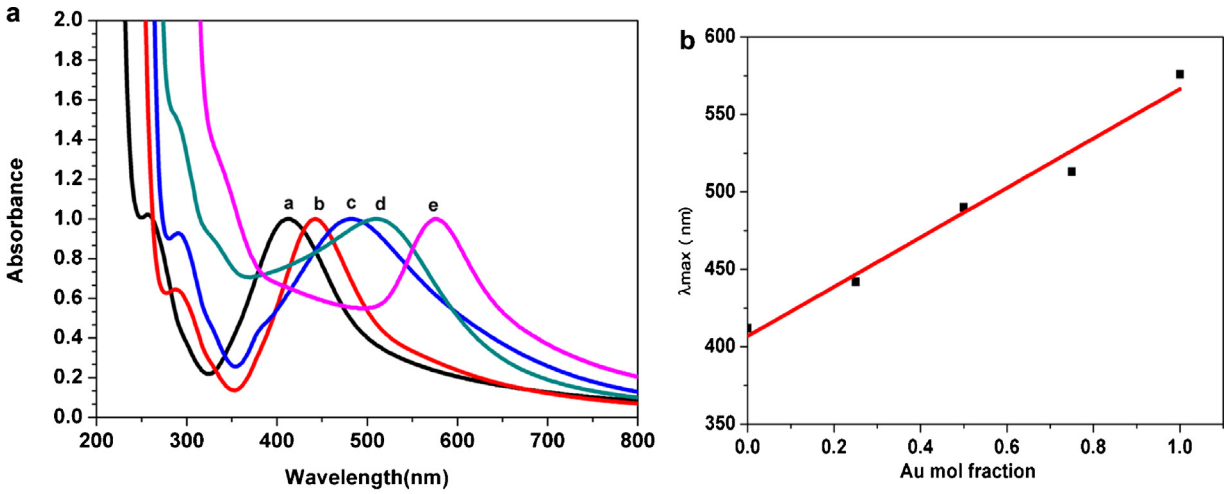

Fig. 1. (a) UV–visible absorption spectra of Au–Ag alloy nanoparticles, a: Ag, b: $Au_{0.25}$:$Ag_{0.75}$, c: $Au_{0.50}$:$Ag_{0.50}$, d: $Au_{0.75}$:$Ag_{0.25}$, e: Au. (b) A linear plot of surface plasmon bands against the mole fractions of Au atoms in alloy nanoparticles.

Table 1
Composition, size, cyclic voltammetry, UV–visible, and photoluminescence spectral data of Ag, Au and Au–Ag alloy NPs.

Molar ratio of NPs	Size (nm)	E_{pa} (V)	E_{pc} (V)	λ_{max} (nm)	λ_{ex} (nm)	λ_{em} (nm)
Ag	3.8 ± 0.80	0.30	−0.67	411	407	443
$Au_{0.25}$:$Ag_{0.75}$	4.1 ± 1.50	0.34	−0.37	443	440	463
$Au_{0.50}$:$Ag_{0.50}$	4.6 ± 1.00	0.37	+0. 15	481	475	513
$Au_{0.75}$:$Ag_{0.25}$	7.0 ± 0.50	0.47	+0. 18	513	500	563
Au	14.4 ± 2.7	0.51	+0. 36	576	575	614

411 nm and 576 nm [Fig. 1a: spectral traces (a) and (e)] respectively in the present investigation.

The UV–visible spectra of the $Au_{0.25}$:$Ag_{0.75}$, $Au_{0.50}$:$Ag_{0.50}$ and $Au_{0.75}$:$Ag_{0.25}$ samples are reproduced in Fig. 1a: spectral traces (b), (c) and (d), which exhibit single absorption maximum at 443, 481, and 513 nm respectively, thus confirming the formation of alloy nanoparticles with only homogeneous composition. The spectra of the alloy nanoparticles did not undergo any change for several months. The surface plasmon absorption of the Au–Ag composite is linearly red-shifted (~170 nm) from that of a monometallic Ag in proportion to the increase in the composition. Au–Ag alloy nanoparticles are very stable in the aqueous phase. The mole fraction of the Au–Ag content indicates that the nanoparticles are alloys rather than core–shell nanoparticles or mixture of monometallic nanoparticles. This is illustrated in Fig. 1b in which the UV–visible absorption maximum is plotted against the mole fraction of Au in the precursor samples. It is known that a physical mixture of monometallic Ag and Au nanoparticles has two absorption peaks corresponding to the monometallic Ag and Au respectively (Kim et al., 2013) (Vide: Supporting information Fig. S2). The core–shell nanoparticles would exhibit the same two absorption peaks (Tang, Yuan, & Chai, 2006), where one increases in absorbance with the increase in the concentration of that component with concomitant decrease in the absorbance of other component. The stability of as synthesized Au and Ag nanoparticles was monitored by UV–visible spectral studies. The SPR band of starch stabilized nanoparticles did not undergo any change either in its position or its intensity even after two months of storage at ambient temperature.

The cyclic voltammograms of GCE modified with Au–Ag alloy nanocoating with the ratio Ag, $Au_{0.75}$:$Ag_{0.25}$, $Au_{0.50}$:$Ag_{0.50}$, $Au_{0.25}$:$Ag_{0.75}$ and Au in PBS medium (pH: 7.4) are reproduced in Fig. 2 and Supporting information (Fig. S3). The AuNPs modified GCE (Au) (Fig. 2a) recorded in the range 0.2–1.0 V shows the broad anodic peak and prominent cathodic peak at 0.51 and 0.36 V respectively. In the case of $Au_{0.50}$:$Ag_{0.50}$ alloy nanoparticle, the anodic peak at 0.37 V and cathodic peak at 0.15 V were observed (Fig. 2b). The redox behavior of the alloy NPs $Au_{0.75}$:$Ag_{0.25}$ and $Au_{0.25}$:$Ag_{0.75}$ is reported in supporting information [Vide: Supporting information: Fig. S3]. The oxidation and reduction peaks appear at 0.34 V, 0.47 V and −0.37 V, 0.18 V respectively (Table 1). But the AgNPs (Ag) modified GCE exhibits the oxidation at E_{pa} = +0.30 V and reduction at E_{pc} = −0.67 V as shown in Fig. 2c.

The oxidation potential (E_{Pa}) gradually increases from 0.30 to 0.51 V and the reduction potential (E_{pc}) also gradually increases from −0.67 to 0.36 V, when the concentration of silver nanoparticles is reduced from 100% to 0% in Au–Ag alloy nanoparticles (Table 1). Moreover the redox potential gradually increases as the size of the NPs is increased from 3.8 to 14.4 nm. These values are comparable to that of the earlier report by Tominaga et al., which indicates the dependency of the redox potential with the size of the Au–Ag alloy NPs as well as the fall in the redox potential with increasing concentration of silver (Raimondi, Scherer, Kcotz, & Wokaun, 2005). Pumera et al. have indicated the size dependent electrochemical behavior of silver (Giovanni & Pumera, 2012) and gold (Bonanni, Pumera, & Miyahara, 2011) nanoparticles. Compton et al. have demonstrated that stripping potential of Ag NPs depends

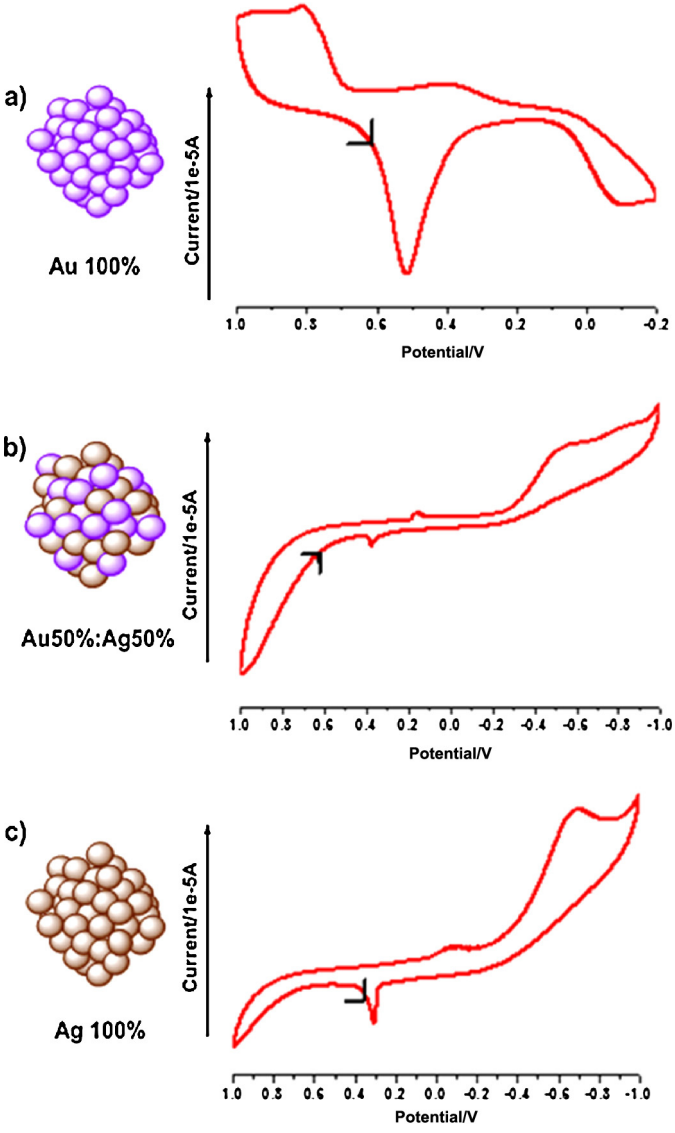

Fig. 2. Voltammograms of Ag, $Au_{0.50}$:$Ag_{0.50}$ and Au nanoparticles modified GCE in a PBS medium.

on the size of the nanoparticles (Jones, Campbell, Baron, & Xiao, 2008).

The redox potential of alloy nanoparticles essentially depends on two factors: size and composition. These two factors may oppose each other in some cases while they have cumulative effect in some other systems. It has been found that if the size of the alloy nanoparticles decreases, anodic potential increases and when the silver content decreases, the oxidation potential also increases (Tominaga et al., 2006). However, in the present investigation it has been found that when the size of the nanoparticle increases, the oxidation potential also increases while the reduction in silver content results in increase in anodic potential. The latter behavior compares well

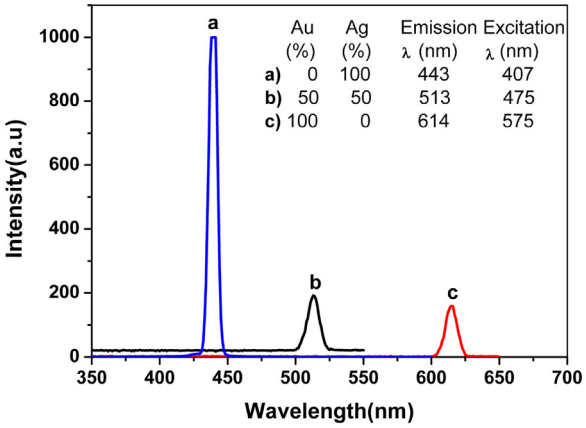

Fig. 3. Emission spectra of Ag, $Au_{0.50}$:$Ag_{0.50}$ and Au nanoparticles.

with that of the literature report, while the former exhibits a reversal in this trend. This observation confirms that the Au–Ag alloy nanoparticles are composed of by homogenous mixture of AgNPs and AuNPs and not by Ag and Au metal domains.

The characteristic photoluminescent behavior of Ag, Au and Au–Ag alloy nanoparticles was observed by measuring fluorescence emission spectra (Fig. 3). The emission maximum of Ag and AuNPs was observed at 443 nm and 614 nm respectively when they were excited at 407 nm and 575 nm respectively. As the molar ratio of Ag decreases, the fluorescence emission maximum undergoes a red shift from 443 to 614 nm along with an increase in excitation wavelength due to synergism (Vide: Supporting information Fig. S4). It has also been observed that when the solutions of metal and alloy NPs were excited at different wavelengths, the emission maximum did not undergo any change. For example, when the solution of Ag was excited at 390, 400 and 407 nm, the λ_{em} was found to be 443 nm while the excitation of $Au_{0.75}$:$Ag_{0.25}$ at 400, 420 and 440 nm resulted in λ_{em} at 463 nm indicating that the alloy NPs is monodisperse. This observation closely resembles that of the silver nanoclusters reported earlier (Ganguly, Pal, Negishi, & Pal, 2013; Shang & Dong, 2008). Millstone et al. have reported the photoluminescence behavior of Au/Cu NP alloys in which the fluorescence of the alloy NPs undergoes bathochromic shift when the concentration of copper increases (Andolina et al., 2013). This is in contrast to the observation made in the case of Au–Ag alloy nanoparticles in which the decreasing concentration of Ag results in increasing red shift. The fluorescence intensity of pure Ag metal is considerably reduced due to the quenching by Au with increase in its concentration, which is similar to the observation made in the earlier report (Ganguly et al., 2013). The fluorescence intensity also decreases with decrease in the Ag concentration in the alloy NPs. The fluorescence maximum depends on the applied potential and it has been demonstrated by Tafel plot (Kaneko, Uosaki, & Kita, 1986; Nag et al., 2012).

When the E_{Pa} of the system increases, the emission wavelength also undergoes a red shift. When the concentration of Ag in the bimetallic alloy is reduced from 100% to 0% the E_{Pa} increases from +0.30 V to +0.51 V with a corresponding increase in the fluorescence emission maximum from 443 nm to 614 nm. The electrochemical studies have clearly established the relationship between the composition and oxidation potential of the NPs. Similar correlation can

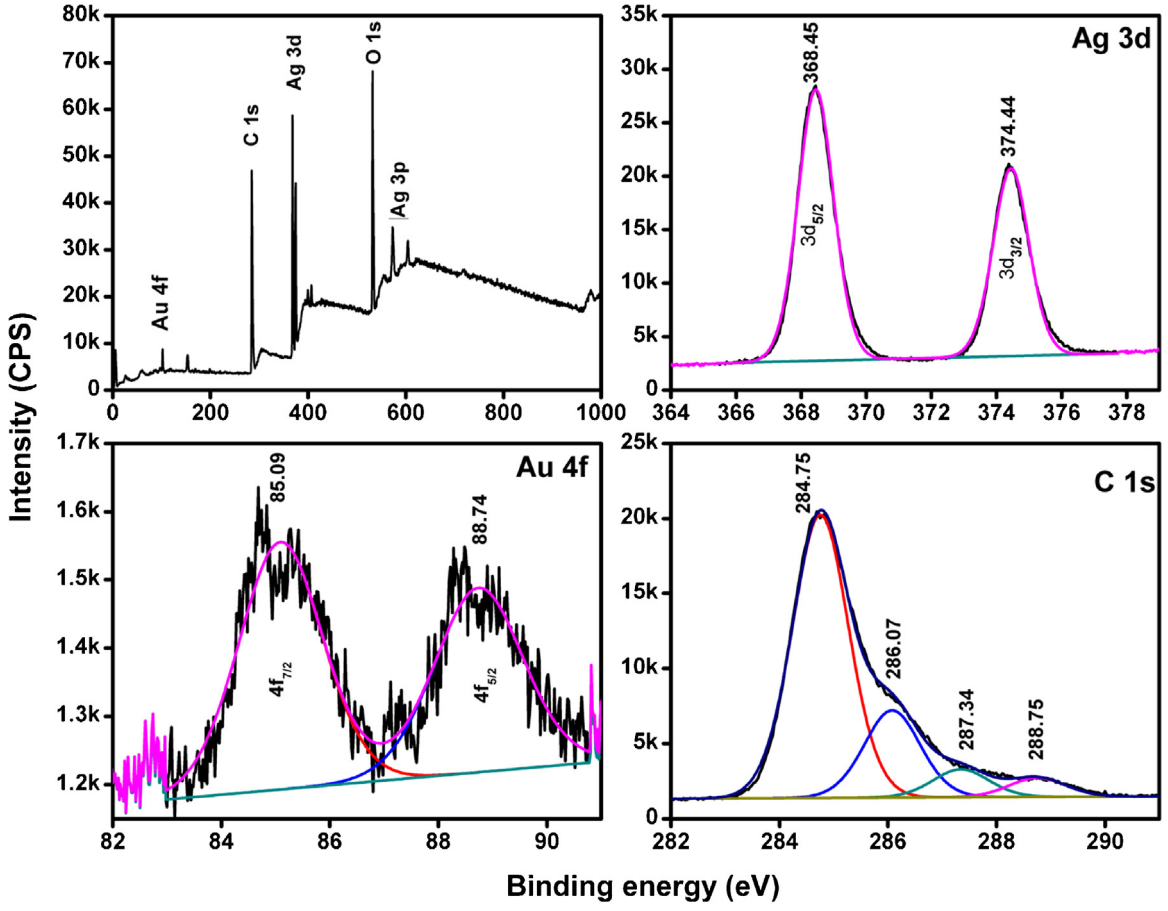

Fig. 4. XPS analysis of Au–Ag alloy nanoparticles ($Au_{0.25}$:$Ag_{0.75}$).

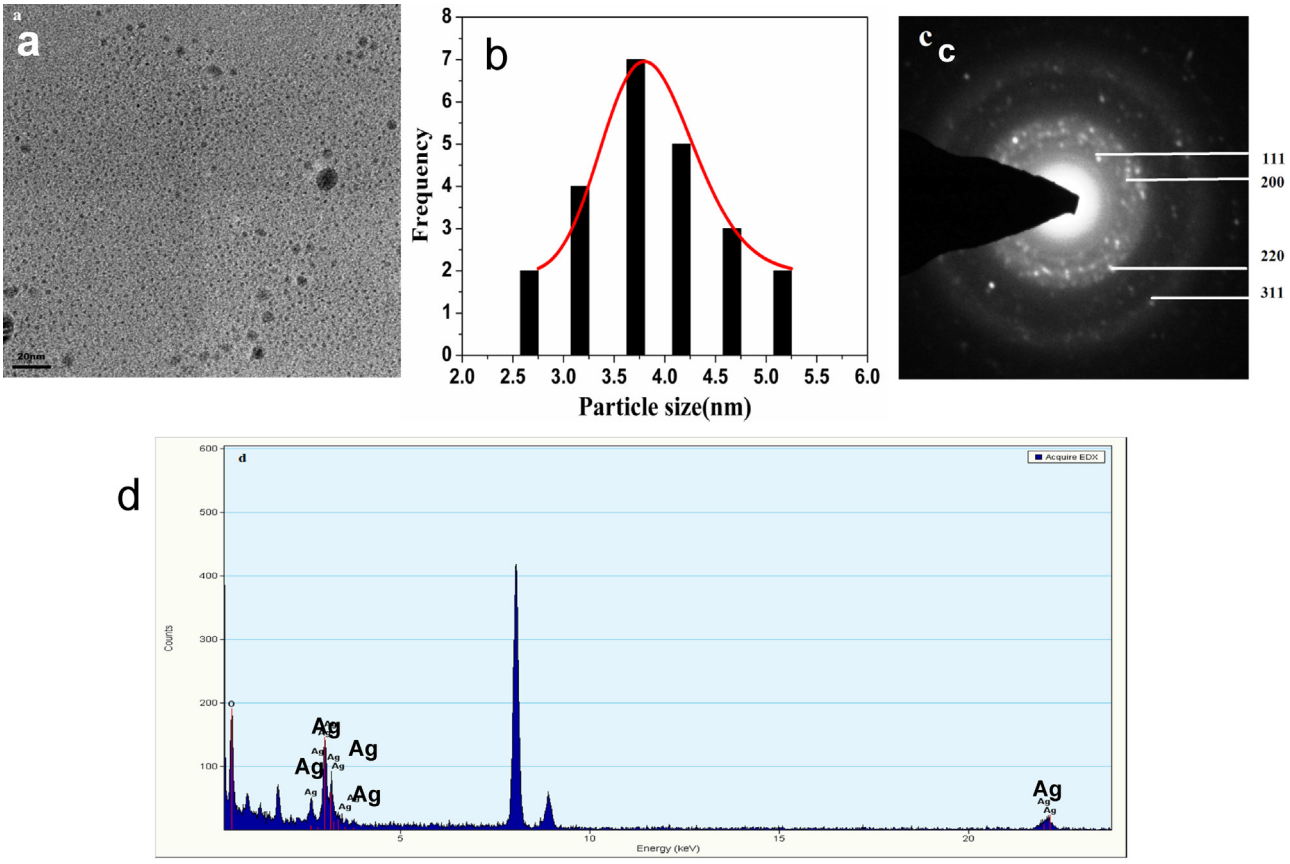

Fig. 5. (a) TEM micrographs of AgNPs (20 nm). (b) Particle size distribution of AgNPs. (c) SAED pattern of AgNPs. (d) EDAX spectrum of AgNPs.

be made between the composition, oxidation potential and emission wavelength [Table 1]. The photoluminescence efficiency of colloidal nanocrystals has also been reported to vary with the zeta potential especially, in the case of Cd/Se colloidal nanocrystals (Nag et al., 2012).

The crystal structure of Au, Ag and their alloy nanoparticles has been further characterized by XRD analysis. The XRD pattern for the synthesized Ag, Au and their alloy nanoparticles are reproduced in supporting information (vide: Supporting Fig. S5). The XRD pattern of Au and Ag synthesized in the present investigation matches with those of earlier reports(JCPDS file nos: 870597and 740526 respectively). The four peaks appearing at $2\theta = 37.97^\circ$, 44.11°, 64.35° and 77.27° correspond to the (1 1 1), (2 0 0), (2 2 0) and (3 1 1) planes, respectively, of the face centered cubic Ag (or Au) particles. Since gold and silver have the same fcc structure and almost the same lattice constant it is difficult to distinguish gold–silver alloy from a mixture of the monometallic phases from XRD pattern (Chen & Chen, 2002; Shankar, Rai, Ahmad, & Sastry, 2004).

The surface alloy composition of Au–Ag alloy NPs was confirmed by X-ray photoelectron spectral analysis. The XPS traces of Au–Ag alloy NPs are shown in Fig. 4. The XPS data for the alloy $Au_{0.25}$:$Ag_{0.75}$ as well as metallic Ag, Au and their peak positions are tabulated (Table 2). Au–Ag alloy nanoparticles show both Au 4f (85.0 eV) and Ag 3d (368.4 eV) peaks in Fig. 4, confirming the bimetallic nature of alloy nanoparticles. The content of Au and Ag within the X-ray penetration depth (3–5 nm) on the surface is quantified by Au 4f and Ag 3d peak areas divided by the respective atomic sensitive factor (ASF) 6.250 and 5.987 which indicates an average composition of 23 atomic% Au and 77 atomic% Ag. In general, the binding energies of alloy nanoparticles exhibit a shift, compared to those of metallic Ag and Au forms, indicating that the two noble metals form alloy nanoparticles rather than individual metal nanoparticles. The XPS binding energies of alloy nanoparticles have been reported by several groups (Kariuki et al., 2004; Srnova-Sloufova, Vickova, Bastl, & Hasslett, 2004). The shift in the peak binding energy is indicative of the formation of alloys. Both Au and Ag bands have been identified (Table 2) which are in agreement with the literature data (Moulder, Stickle, Sobol, & Bomben, 1995). The analysis of XPS spectra confirms the presence of starch (C1s) as a capping agent of the Au–Ag alloy nanoparticles, which prevents their aggregation (Fig. 4). The C1s spectrum shows peaks corresponding to C (CH_2) at 284.7 eV, C—O at 286.0 eV, O—C—O at 287.3 eV and O=C—O at 288.7 eV.

Table 2
XPS peak positions (BE/eV) for Au–Ag NPs.

Nanoparticles	Au ($4f_{7/2}$)	Ag ($3d_{5/2}$)
Au	84.0	–
Ag	–	368.0
Au (0.25):Ag (0.75)	85.0	368.4

BE, binding energy; eV, electron volts.

The nature of the metal nanoparticles has been analyzed by TEM and selected area electron diffraction pattern (SAED) studies. The representative TEM images recorded from carbon coated copper grid of the AgNPs prepared by the reduction of Ag^+ ions in starch by INH are reproduced (Fig. 5a). The particles are polydisperse in nature with an average size of 3.8 ± 0.8 nm (Fig. 5b). The SAED for AgNPs and the ring pattern are indexed to the 1 1 1, 2 0 0, 2 2 0 and 3 1 1 Bragg reflections from the fcc structure of silver (Fig. 5c). The EDAX spectrum of AgNPs shows peaks around 3.4 keV, which correspond to the binding energies of silver thus confirming the formation of metallic AgNPs (Fig. 5d).

The TEM micrograph for AuNPs is shown in Fig. 6a. The nanoparticles are spherical and monodisperse with diameter in the range

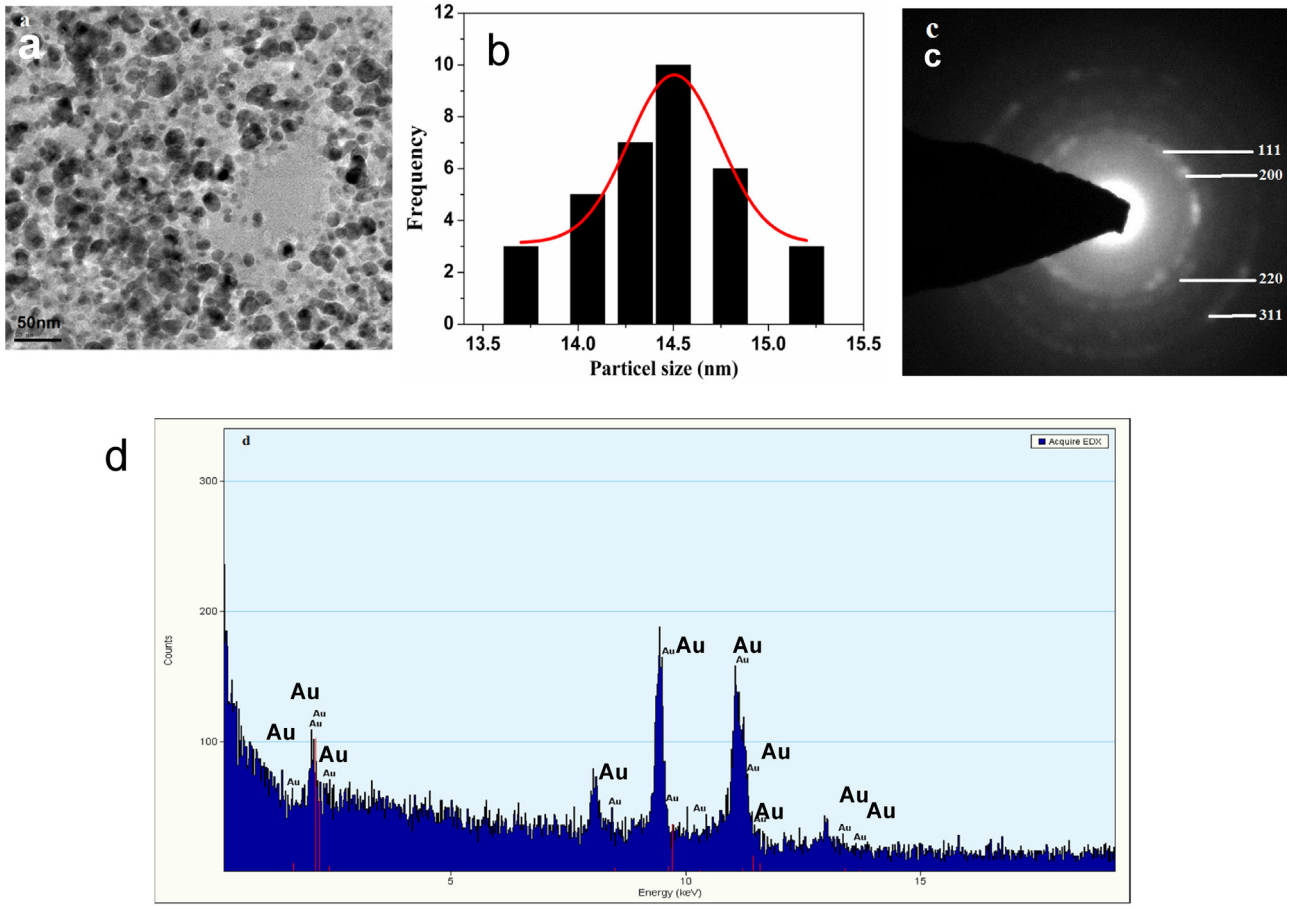

Fig. 6. (a) TEM micrographs of AuNPs (50 nm). (b) Particle size histogram of AuNPs. (c) SAED pattern of AuNPs. (d) EDAX spectrum of AuNPs.

of 14.4 ± 2.7 nm (Fig. 6b). The SAED for AuNPs and the ring pattern are indexed to the 1 1 1, 2 0 0, 2 2 0 and 3 1 1 Bragg reflections from the fcc structure of gold (Fig. 6c). The EDAX spectrum of AuNPs is shown in Fig. 6d. The peaks around 1.8 and 10.8 keV correspond to the binding energies of AuNPs, indicating that the resultant product is metallic AuNPs.

The TEM indicates the size and shape of the alloy nanoparticles. Fig. 7a shows the TEM micrograph recorded at equimolar ratio of Au–Ag alloy NPs. The average size of the alloy NPs is 4.6 ± 1.0 nm; Au: 0.50 (Fig. 7b) and they are spherical in shape (Table 1). The SAED pattern of $Au_{0.50}$:$Ag_{0.50}$ confirms that the alloy NPs formed are crystalline in nature and they belong to fcc lattice (Fig. 7c). Both Au and Ag adapt an fcc structure and have very close crystal lattice parameters. Hence it would be very difficult to observe any shift in the position of the rings from those of individual Au or Ag NPs. The EDAX analysis suggests the Au–Ag mole ratio of the sample with an elemental composition of Au (50%) and Ag (50%) (Fig. 7d). The size of alloy nanoparticles is less than 10 nm, which is smaller than that of Ag–Au alloy prepared in aqueous solution as reported earlier (Kim et al., 2013). The TEM images of Au–Ag alloy nanoparticles did not show either a dense core or a light shell, which is typical for core–shell structure. The TEM micrographs recorded at different molar ratios of Au–Ag alloy NPs and the average size of the alloy NPs are 4.1 ±1.5 nm; Au: 0.25 and 7.0 ± 0.5 nm; Au: 0.75 nm and they are spherical in shape (Vide: Supporting Fig. S6) and (Table 1).

3.1. Catalytic activity of Au, Ag, and Au–Ag alloy nanoparticles

The catalytic efficiency of Au–Ag alloy nanoparticles for the reduction of mono and trinitrophenol systems has been investigated. In a typical bimetallic catalytic reduction in the present investigation, upon the addition of $NaBH_4$ to the aqueous 4-nitrophenol (4NP), nitrophenolate ion is formed immediately (Li et al., 2012) which shows red shift in the UV–visible absorption band from 317 to 400 nm (Fig. 8a). In the absence of any catalyst, the thermodynamically favorable reduction of 4-NP (E° for 4-NP/4-AP = −0.76 V and H_3BO_3/BH_4^- = −1.33 V versus NHE) was not observed and the peak due to 4-nitrophenolate ion at 400 nm remains unaltered even for a couple of days (Mrinmoyee & Tarasankar, 2011; Chap. 2). However, immediately after adding a small amount of catalyst Ag or Au into the reaction system, the intensity of the absorption band at 400 nm successively decreases with increasing reaction time and simultaneously a new band appears at 300 nm indicating the formation of 4-AP (Fig. 8b).

The product conversion is fast (12 min) in the presence Au (100%) (Vide: Supporting information Fig. S7) catalyst when compared to that of Au (0%) (40 min) (Vide: Supporting information Fig. S8). However, the reaction is completed within 30 min in the presence of bimetallic alloy nanoparticles Au (50%):Ag (50%). The catalyst appears to have marginal influence on the reduction of picric acid (PA) system and the reduction occurs within 5 min with or without the addition of catalyst. The electron withdrawing effect of the three nitro groups and resonance structure play an important role in the process of strong reduction. The reduction of one of the nitro groups to amino group activates the benzene ring by electron donation. However, immediately after adding a small amount of $NaBH_4$ to the reaction system, the disappearance of 355 nm peak indicates the complete reduction of nitro compound (Fig. 8c).

The kinetic rate constants of the Au, Au–Ag alloys and Ag nanoparticles are reproduced in supporting information (Vide:

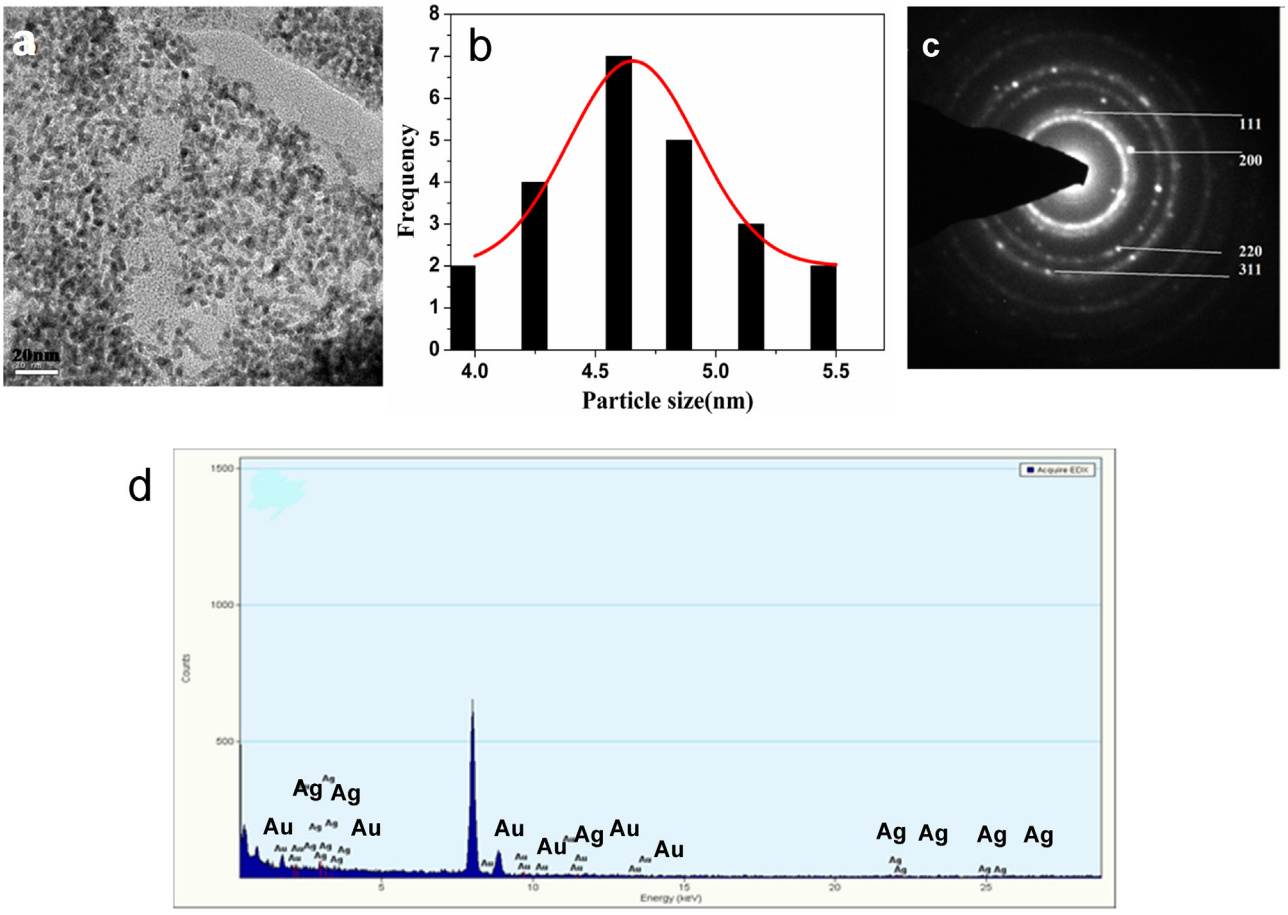

Fig. 7. (a) TEM images of $Au_{0.50}$:$Ag_{0.50}$ alloy NPs (20 nm). (b) Particle size histogram of $Au_{0.50}$:$Ag_{0.50}$ alloy NPs. (c) SAED pattern of $Au_{0.50}$:$Ag_{0.50}$ alloy NPs (b) EDAX spectrum of $Au_{0.50}$:$Ag_{0.50}$ alloy NPs

Supporting Fig. S9). The rate constant of Au nanoparticles is $2.884 \times 10^{-3}\ s^{-1}$, which is significantly higher than those of Au–Ag alloy nanoparticles ($1.7606 \times 10^{-3}\ s^{-1}$, $1.3368 \times 10^{-3}\ s^{-1}$ and $1.0564 \times 10^{-3}\ s^{-1}$ for $Au_{0.75}$:$Ag_{0.25}$, $Au_{0.50}$:$Ag_{0.50}$ and $Au_{0.25}$:$Ag_{0.75}$ particles respectively) as well as that of AgNPs ($0.6880 \times 10^{-3}\ s^{-1}$). The rate constant for the reduction exponentially increases from $0.6880 \times 10^{-3}\ s^{-1}$(Ag) to $2.884 \times 10^{-3}\ s^{-1}$(Au) as the gold content was increased in the Au–Ag alloy nanoparticles indicating that Au could be much more efficient than Ag for the electron transfer from BH_4^- ion to 4-nitrophenol (Vide: supporting information Table: S10). The reduction of 4-nitrophenol in the presence of $NaBH_4$ and Au–Ag alloy nanoparticles was investigated and it was found that the rate constant for the reduction exponentially increases from Ag to Au as the Au content was increased in Au–Ag alloy nanoparticles (Shin, Dohnalkova, & Lin, 2010). However, there is no definite correlation between the composition of the alloy nanoparticles, size and rate. The percentage of Au in Au–Ag alloy NPs and their corresponding alloy nanoparticle size can vary either linearly (Mallin & Murphy, 2002), inversely (Kariuki et al., 2004) or at random (Pal, Shah, & Devi, 2007) depending on the method of preparation. The size of the Au–Ag alloy NPs in the present investigation increases with the increase in the Au content in the alloy NPs.

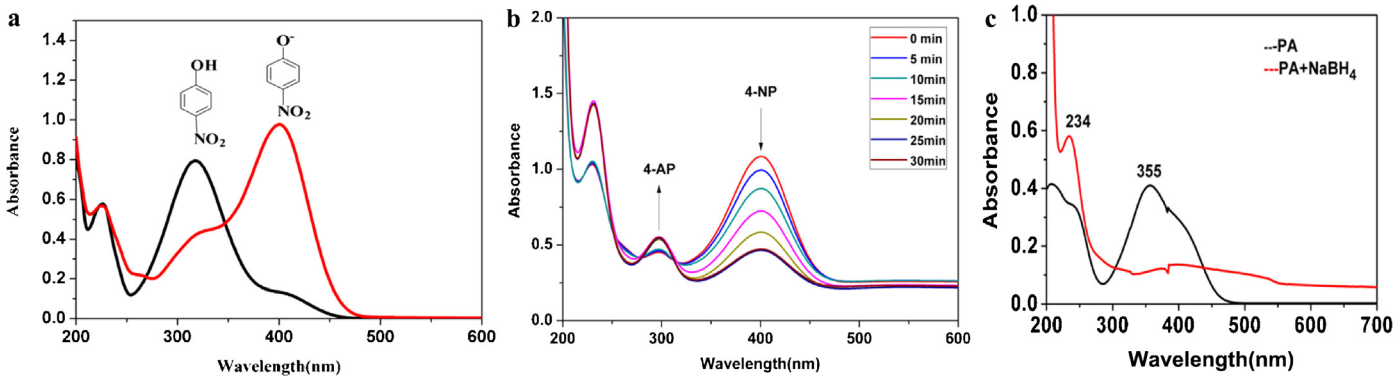

Fig. 8. (a) UV–visible absorption spectra of 4-nitrophenol and 4-nitrophenolate ion. (b) UV–vis absorption spectrum of 4-nitrophenol in the presence of $NaBH_4$ and catalyst ($Au_{0.50}$:$Ag_{0.50}$) at different time intervals. (c) UV–visible absorption spectrum of picric acid (black) and after the addition of $NaBH_4$ (red). (For interpretation of the references to color in text, the reader is referred to the web version of the article.)

4. Conclusions

The rapid and green synthesis of stable silver, gold and Au–Ag alloy nanoparticles has been achieved using anti-TB drug INH as a reducing agent. The formation of homogeneous alloy nanoparticles was confirmed by UV–visible absorption spectroscopy, CV, fluorescence, TEM and XPS measurements. The alloy nanoparticles were synthesized within a short period using environmentally benign chemicals. The TEM analysis shows that the mean particle size increases from 3.8 ± 0.8 nm for (Ag) to 14.4 ± 2.7 nm for (Au) while the size of Au–Ag alloy NPs is found to be 4.1 ± 1.5, 4.6 ± 1.0, and 7.0 ± 0.5 nm, respectively. The surface plasmon band displays a red shift with the increase of Au% in the bimetallic nanoparticles, which confirms the formation Au–Ag alloy nanoparticles. When the Ag content in the alloy decreases, the size of the nanoparticles increases and as a result of which not only the oxidation potential increases but also the emission maximum undergoes a bathochromic shift from 443 to 614 nm. The rate of conversion of 4-NP to 4-AP is significantly enhanced by the bimetallic catalyst when $NaBH_4$ was employed as a reducing agent. However, the role of catalyst in the reduction of picric acid was found to be only marginal.

Acknowledgements

We thank National Center for Nanoscience and Nanotechnology (NCNST), University of Madras for TEM and XPS studies. The financial support by the Indian Council of Medical Research (ICMR), New Delhi is gratefully acknowledged.

Appendix A. Supplementary data

Supplementary material related to this article can be found, in the online version, at http://dx.doi.org/10.1016/j.carbpol.2014.04.105.

References

Anandan, S., Grieser, F., & Ashokkumar, M. (2008). Sonochemical synthesis of Au–Ag core–shell bimetallic nanoparticles. *Journal of Physical Chemistry C*, *112*, 15102–15109.

Andolina, C. M., Dewar, A. C., Smith, A. M., Marbella, L. E., Hartmann, M. J., & Millstone, J. E. (2013). Photoluminescent gold–copper nanoparticle alloys with composition-tunable near-infrared emission. *Journal of the American Chemical Society*, *135*, 5266–5269.

Aryal, S., Remant Bahadur, K. C., Dharmaraj, N., Bhattarai, N., Kim, C. H., & Kim, H. Y. (2006). Spectroscopic identification of S–Au interaction in cysteine capped gold nanoparticles. *Spectrochimica Acta A*, *63*, 160–163.

Bonanni, A., Pumera, M., & Miyahara, Y. (2011). Influence of gold nanoparticle size (2–50 nm) upon its electrochemical behavior: An electrochemical impedance spectroscopic and voltammetric study. *Physical Chemistry Chemical Physics*, *13*, 4980–4986.

Carosi, G., & Matteelli, A. (1996). Prophylaxis for tuberculosis in Europe – Ongoing research. *Clinical Infections Disease*, *22*, 55–60.

Chen, D. H., & Chen, C. J. (2002). Formation and characterization of Au–Ag bimetallic nanoparticles in water-in-oil microemulsions. *Journal of Material Chemistry*, *12*, 1557–1562.

Chen, Y. H., & Yeh, C. S. (2001). New approach for the formation of alloy nanoparticles: Laser synthesis of gold–silver alloy from gold–silver colloidal mixtures. *Chemical Communications*, *4*, 371–372.

Corbett, J. F. (1999). An historical review of the use of dye precursors in the formulation of commercial oxidation hair dyes. *Dyes and Pigments*, *41*, 127–136.

Ganguly, M., Pal, A., Negishi, Y., & Pal, T. (2013). Synthesis of highly fluorescent silver clusters on gold(I) surface. *Langmuir*, *29*, 2033–2044.

Giovanni, M., & Pumera, M. (2012). Size dependant electrochemical behavior of silver nanoparticles with sizes of 10, 20, 40, 80 and 107 nm. *Electroanalysis*, *24*, 615–617.

Hostetler, M. J., Zhong, C. J., Yen, B. K. H., Anderegg, J., Gross, S. M., Evans, N. D., et al. (1998). Stable, monolayer-protected metal alloy clusters. *Journal of the American Chemical Society*, *120*, 9396–9397.

Hussain, J. I., Kumar, S., Hashmi, A. A., & Khan, Z. (2011). Silver nanoparticles: Preparation characterization and kinetics. *Advanced Materials Letters*, *2*, 188–194.

Jones, S. E. W., Campbell, F. W., Baron, R., & Xiao, L. (2008). Particle size and surface coverage effects in the stripping voltammetry of silver nanoparticles: Theory and experiment. *Journal of Physical Chemistry C*, *112*, 17820–17827.

Kaneko, S., Uosaki, K., & Kita, H. (1986). Accumulation layer formation at N-gallium arsenide/electrolyte interface: Photoluminescence probe of the kinetic barrier for hydrogen evolution reaction. *Journal of Physical Chemistry*, *90*, 6654–6657.

Kariuki, N. N., Luo, J., Maye, M. M., Hassan, S. A., Menard, T., Richard Naslund, H., et al. (2004). Composition-controlled synthesis of bimetallic gold–silver nanoparticles. *Langmuir*, *20*, 11240–11246.

Kim, W. J., Kim, S., Kim, A. R., & Yoo, D. J. (2013). Direct detection system for *Escherichia coli* using Au–Ag alloy microchips. *Industrial and Engineering Chemistry Research*, *52*, 7282–7288.

Kruger–Thiemer, E. (1955). Chemismus der Isoniazid Spaltung Durch Hämin. *Naturwissenschaften*, *42*, 47–48.

Lee, I., Han, S., & Kim, K. (2001). Production of Au–Ag Alloy nanoparticles by laser ablation of bulk alloys. *Chemical Communications*, *18*, 1782–1783.

Li, T., Chattopadhyay, S., Shibata, T., Cook, R. E., Miller, J. T., Suthiwangcharoen, N., et al. (2012). Synthesis and characterization of Au-core Ag-shell nanoparticles from unmodified apoferritin. *Journal of Material Chemistry*, *22*, 14458–14464.

Link, S., Burda, C., Wang, Z. L., & El-Sayed, M. A. (1999). Electron dynamics in gold and gold–silver alloy nanoparticles: The influence of a nonequilibrium electron distribution and the size dependence of the electron–phonon relaxation. *Journal of Chemical Physics*, *111*, 1255–1264.

Link, S., Wang, Z. L., & El-Sayed, M. A. (1999). Alloy formation of gold–silver nanoparticles and the dependence of the plasmon absorption on their composition. *Journal of Physical Chemistry B*, *103*, 3529–3533.

Liz-Marzan, L. M., & Philipse, A. P. (1995). Stable hydrosols of metallic and bimetallic nanoparticles immobilized on imogolite fibers. *Journal of Physical Chemistry*, *99*, 15120–15128.

Mallin, M. P., & Murphy, C. J. (2002). Solution-phase synthesis of sub-10 nm Au–Ag alloy nanoparticles. *Nano Letters*, *2*, 1235–1237.

Magria, D. C., & Prasanna de Silva, A. (2010). From PASS 1 to YES to AND Logic: Building parallel processing into molecular logic gates by sequential addition of receptors. *New Journal of Chemistry*, *34*, 476–481.

Moulder, J. F., Stickle, W. F., Sobol, P. E., & Bomben, K. D. (1995). Handbook of X-ray photoelectron spectroscopy. In J. Chastain, & R. C. King (Eds.), *Physical electronics*. Minnesota USA: Eden Prairie.

Mrinmoyee, B., & Tarasankar, P. (2011). In B. Chauhan (Ed.), *Hybrid nanomaterials* (pp. 23–64). Hoboken, NJ: John Wiley & Sons, Inc.

Nag, A., Chung, D. S., Dolzhnikov, D. S., Dimitrijevic, N. M., Chattopadhyay, S., Shibata, T., et al. (2012). Effect of metal ions on photoluminescence, charge transport, magnetic and catalytic properties of all-inorganic colloidal nanocrystals and nanocrystal solids. *Journal of the American Chemical Society*, *134*, 13604–13615.

Naik, R. R., Stringer, S. J., Agarwal, G., Jones, G. S., & Stone, M. O. (2002). Biomimetic synthesis and patterning of silver nanoparticles. *Nature Materials*, *1*, 169–172.

Okazaki, K. I., Kiyama, T., Hirahara, K., Tanaka, N., Kuwabata, S., & Torimoto, T. (2008). Single-step synthesis of gold–silver alloy nanoparticles in ionic liquids by a sputter deposition technique. *Chemical Communications*, *6*, 691–693.

Pal, A., Shah, S., & Devi, S. (2007). Preparation of silvergold and silver–gold bimetallic nanoparticles in W/O microemulsion containing tritonX-100. *Colloids and Surfaces A: Physicochemical and Engineering Aspects*, *302*, 483–487.

Raimondi, F., Scherer, G. G., Kcotz, R., & Wokaun, A. (2005). Nanoparticles in energy technology: Examples from electrochemistry and catalysis. *Angewandte Chemie International Edition*, *44*, 2190–2209.

Raveendran, P., Fu, J., & Wallen, S. L. (2003). Completely "green" synthesis and stabilization of metal nanoparticles. *Journal of the American Chemical Society*, *125*, 13940–13941.

Senapati, S., Ahmad, A., Khan, M. I., Sastry, M., & Kumar, R. (2005). Extracellular biosynthesis of bimetallic Au–Ag alloy nanoparticles. *Small*, *1*, 517–520.

Sharghi, H., Eskandari, M. M., & Ghavami, R. (2004). A facile converison of epoxides to halohydrins with elemental halogen using isonicotinic hydrazide. *Journal of Molecular Catalysis A – Chemical*, *215*, 55–62.

Shang, L., & Dong, S. (2008). Facile preparation of water-soluble fluorescent silver nanocluster using a polyelectrolyte template. *Chemical Communications*, 1088–1090.

Shankar, S. S., Rai, A., Ahmad, A., & Sastry, M. (2004). Rapid synthesis of Au, Ag, and bimetallic Au core–Ag shell nanoparticles using neem (*Azadirachta indica*) leaf broth. *Journal of Colloid and Interface Science*, *275*, 496–502.

Shin, Y., Dohnalkova, A., & Lin, Y. (2010). Preparation of homogeneous gold–silver alloy nanoparticles using the apoferritin cavity as a nanoreactor. *Journal of Physical Chemistry C*, *114*, 5985–5989.

Srnova-Sloufova, I., Vickova, B., Bastl, Z., & Hasslett, T. L. (2004). Bimetallic (Ag)Au nanoparticles prepared by the seed growth method: Two-dimensional assembling, characterization by energy dispersive X-ray analysis, X-ray photoelectron spectroscopy, and surface enhanced raman spectroscopy, and proposed mechanism of growth. *Langmuir*, *20*, 3407–3415.

Tang, D., Yuan, R., & Chai, Y. (2006). Ligand-functionalized core/shell Ag@Au nanoparticles label-free amperometric immun-biosensor. *Biotechnology and Bioengineering*, *94*, 996–1004.

Teo, B. K., Keating, K., & Kao, Y. H. (1987). Observation of plasmon frequency in the optical spectrum of $Au_{18}Ag_{20}$ cluster: The beginning of the collective phenomenon characteristics of the bulk? *Journal of the American Chemical Society*, *109*, 3494–3495.

Tominaga, M., Shimazoe, T., Nagashima, M., Kusuda, H., Kubo, A., Kuwahara, Y., et al. (2006). Electrocatalytic oxidation of glucose at gold–silver alloy, silver and gold nanoparticles in an alkaline solution. *Journal of Electroanalytical Chemistry*, *590*, 37–46.

Wang, A. Q., Liu, J. H., Lin, S. D., Lin, T. S., & Mou, C. Y. (2005). A novel efficient Au–Ag alloy catalyst system: Preparation, activity, and characterization. *Journal of Catalysis*, *233*, 186–197.

Winder, F. (1956). Liberation of peroxide in the breakdown of isoniazid. *American Review of Tuberculosis*, *73*, 779–780.

Zhang, H., Zhang, Y., Wei, X., Du, X., & Li, Q. (2009). Novel spectrophotometric method for the determination of isoniazid using Cu (II) as spectroscopic prone ion. *Chinese Journal of Chemistry*, *27*, 518–522.